Surfaces and Interfaces 46 (2024) 103954

Contents lists available at ScienceDirect

Surfaces and Interfaces

journal homepage: www.sciencedirect.com/journal/surfaces-and-interfaces

Photoluminescent and superhydrophobic nanocomposites of perovskite nanocrystals

Sema Karabel Ocal [a,b,c], Nusret Çelik [b,c], M. Serdar Onses [b,c,d,*], Evren Mutlugun [a,d,*]

[a] Department of Electrical and Electronics Engineering, Abdullah Gul University, Kayseri, 38080, Turkey
[b] Department of Materials Science and Engineering, Erciyes University, Kayseri, 38039, Turkey
[c] ERNAM - Erciyes University Nanotechnology Application and Research Center, Kayseri, 38039, Turkey
[d] UNAM–National Nanotechnology Research Center, Institute of Materials Science and Nanotechnology, Bilkent University, Ankara 06800, Turkey

ARTICLE INFO

Keywords:
Nanocrystals
Perovskites
Superhydrophobic

ABSTRACT

Perovskite nanocrystals (PNCs) have found extensive utility across diverse technological applications in optoelectronics; nevertheless, their susceptibility to environmental instability poses a significant constraint on their practicality. Within this investigation, we present a novel and facile approach for the development of highly stable superhydrophobic PNCs. These engineered superhydrophobic perovskite nanocrystal composites, referred to as HSNPs@PNCs, demonstrate remarkable optoelectronic attributes, provided that their inherent instability can be effectively mitigated. HSNPs@PNCs manifest an impressive water contact angle of 172° and an exceedingly low sliding angle of 1°, thus showcasing their exceptional superhydrophobicity. Of particular note is the extraordinary stability exhibited by HSNPs@PNCs despite aqueous environments, thermal fluctuations, and UV exposure. Remarkably, even after a prolonged 30-day immersion in water, this nanocomposite maintains an outstanding emission efficiency of 75 %. Furthermore, the method of application through a spray deposition technique circumvents sample size limitations, thereby amplifying their suitability for industrial applications. Moreover, this study extends the practicality of HSNPs@PNCs by enabling their homogeneous coating onto various surfaces such as glass, fabric, and aluminum, yielding luminescent superhydrophobic surfaces. This approach liberates the substrates from constraints, significantly broadening the potential spectrum of applications for these materials within diverse industrial and technological domains.

1. Introduction

Perovskite nanocrystals (PNCs) have drawn significant attention due to outstanding properties such as narrow spectral bandwidth, high quantum yield (QY) and easily tunable emissions, high color purity, and low-cost processing techniques [1,2]. Recently, because of this unique properties, PNCs have been used in applications such as light-emitting diodes, White-light-emitting diodes, lasers, solar cells, fuel cells, water electrolysis, renewable energy, photodetectors, bioimaging [3–13]. However, practical applications are hindered by the poor stability of PNCs. Due to their ionic properties and low surface energies [14], PNCs are very sensitive under environmental conditions (temperature, humidity, light, oxygen) and lose their fluorescent properties under extreme conditions [14–18].

To overcome the instability of PNCs, researchers have studied a variety of approaches, such as using water resistant ligands, surface passivation, core-shell structure, encapsulation polymers, and inorganic compounds [19–29]. Most inorganic materials have straightforward stability, super mechanical properties, and excellent thermal stability than most organic materials [30,31]. Thus, some particular inorganic materials, such as Al_2O_3, CaF_2, TiO_2, SiO_2, and zeolites have been commonly used to enhance the stability of PNCs [32–35]. For example, Wei et al. increased the stability of PNCs against extreme conditions by encapsulating the PNCs with CaF_2[34].Wang et al. integrated PNCs into porous silica for superior performance in thermal and optical environments [36]. However, oxygen and moisture can penetrate the PNCs in the porous structure of the silica [36] . SiO_2 based coatings have been widely used to show the superior stability of PNCs against water [37]. Hu et al. improved the water and thermal stability of PNCs using anhydrous silica spheres [38]. Although there are various works in the literature on the stability of perovskites in different conditions, here we present the development of perovskite nanocrystals in their

* Corresponding authors at: Department of Electrical and Electronics Engineering, Abdullah Gul University, Kayseri, 38080, Turkey.
E-mail addresses: onses@erciyes.edu.tr (M.S. Onses), evren.mutlugun@agu.edu.tr (E. Mutlugun).

https://doi.org/10.1016/j.surfin.2024.103954
Received 26 October 2023; Received in revised form 16 January 2024; Accepted 21 January 2024
Available online 28 January 2024

superhydrophobic composites form and report a comprehensive study on their stability, with an extensive focus through thermal, water, storage and UV exposure.

An attractive route to improve the water stability of PNCs involves the exploitation of superhydrophobic coatings. These coatings exhibit water contact angles higher than 150° and roll off angles less than 10° Superhydrophobic surfaces are formed by combining hierarchical structures with low surface energy chemicals on the same platform [39–42]. The strategy in topographic structures modified with low surface energy molecules is known as the Cassie state. In this state, the air trapped between the structures keeps the water on its surface, providing low sliding angles, and ensuring that the surface does not get wet [43,44]. The ability to repel water enables the fabrication of self-cleaning [45], anti-fouling [46], anti-corrosion [47], and anti-icing surfaces [48], and found applications that range from biomedical [49] to food-packaging applications [50].

To improve the stability of PNCs, surface properties have been enhanced with organic ligands and hydrophobic matrices in an in-situ approach [16,51,52]. Wang et al. showed that using phase separation, they realized highly shiny PNC-polymer composites with superhydrophobic micro/nanostructured surfaces. These composites have a contact angle of 152°[53]. You et al. showed that PNCs are protected from water degeneration by encapsulating PNCs with superhydrophobic aerogels with a contact angle of 160°[54]. Hsieh et al. have developed composite materials with water resistance and thermal stability [14]. The QY of the composite reduced to 50 % of the initial value after 14 days. Chen et al. synthesized the $CsPbBr_3$wrapped with SiO_2 aerogels [17] . This composite provided protection against 40 min of ultrasonic treatment in water and exhibited thermal and light stability. The water contact angle was not very high, which is an indication of insufficient stability against water. In addition, a photoluminescence retention above 90 % could not be achieved when heated at temperatures ≥70 °C.

In this study, we present a versatile and simple approach to prepare superhydrophobic PNCs with very high contact angles. PNCs and alkylsilane modified hydrophobic silica nanoparticles (HSNPs) were prepared separately and then mixed to generate HSNPs@PNCs. This approach was chosen to benefit from the optimized synthesis of both HSNPs and PNCs without degrading their wetting and photophysical properties, respectively. The resulting composite materials have been applied on various surfaces through spray deposition technique that eludes sample size limitations, thereby amplifying their suitability for industrial applications. Compared to bare PNCs, HSNPs@PNCs displayed superior performance in terms of waterproofing after 30 days of ultrasonic mixing, maintaining its efficiency above 75 %. In addition, thanks to the water-repellent (CA∼172°) feature of superhydrophobic HSNPs@PNCs films, water droplets can splash out and surface contaminants can be removed with its self-cleaning feature. In thermal stability, it has preserved over 90 % of its initial efficiency at a high temperature value of 70 °C. For this reason, the reported strategy offers great opportunities for future studies of optoelectronic devices due to its easy, scalable, cost-effective, and long-term stability to produce highly stable superhydrophobic luminescent films.

2. Experimental section

2.1. Materials

Cesium carbonate (Cs2CO3; 99.9 %), lead (II) bromide (PbBr2; 99 %), lead(II), Iodide (PbI2; 90 %), Lead(II) Chloride (PbCl2; 90 %), SiO_2 nanoparticles (11 nm), 1-Octadecene (ODE; 90 %), Oleic acid (OA; 90 %), Oleylamine (OAm; 90 %), hexane (90 %) and acetone (90 %) were purchased from Sigma-Aldrich. Ethyl acetate (99.5 %) and dodecyltrichlorosilane were purchased from Aladdin and Gelest, respectively.

2.2. Preparation of cesium oleate (Cs-OA) precursor

ODE (20 mL), Cs_2CO_3 (0.4 g), and OA (1.55 mL) were mixed in a three-neck flask under vacuum at 120 °C for 60 min. The temperature of the solution was raised to 150 °C and kept at this temperature until all Cs_2CO_3 was completely dissolved in the ODE. The Cs-oleate precursor solution was stored in a glovebox, after cooling to room temperature.

2.3. Synthesis of PNCs

0.188 mmol of $PbBr_2$ and 5 mL of ODE were mixed in a 25 mL flask and kept under vacuum at room temperature for 30 min, then stirred at 120 °C under an atmosphere of argon gas. 0.5 mL of OAm and 0.5 mL of OA were added to the solution and incubated at 120 °C for 10 min. Next, the temperature of the solution was raised to 180 °C and 0.4 mL of Cs-oleate was quickly injected into the solution, then cooled to room temperature within 5 s.

To purify the as-synthesized material, the mixture was added to a 50 mL centrifuge tube and centrifuged at 5000 rpm for 3 min and the supernatant was discarded. 300 μL of hexane was added to precipitate and the PNCs were dispersed. Next, the solution was centrifuged again at 5000 rpm for 3 min and the supernatant was removed and finally 300 μL of hexane, 25 μL of OA and 25 μL of OAm and 600 μL of acetone were added. The mixture was centrifuged at 5000 rpm for 3 min and the supernatant was discarded and the PNCs were dissolved in fresh hexane.

Blue- and red-emitting PNCs were also synthesized via the exact same synthesis steps. Mixtures of $PbBr_2$−$PbCl_2$ (0.094 mmol of $PbBr_2$ + 0.094 mmol of $PbCl_2$) and $PbBr_2$−PbI_2 (0.075 mmol of $PbBr_2$ + 0.113 mmol of PbI_2) were used for blue and red emitting PNCs, respectively.

2.4. Functionalization of silica nanoparticles

2 g of hydrophilic silica nanoparticles were added to 40 mL of toluene and mixed with a magnetic stirrer. After homogeneous mixing, 1 mL of dodecyltrichlorosilane was added slowly into silica nanoparticles dispersed in toluene and stirred for 3 h. HSNPs were separated from the solvent by centrifugation at 4000 rpm for 15 min and drying at 80 °C for 12 h.

2.5. Preparation of HSNPs@PNCs

The prepared PNCs solution (2 mL) was added to a flask containing 0.2 g of HSNPs and stirred in hexane for 2 h and then nanocomposite powder was obtained by drying in a vacuum for 1 h. Then the dried HSNPs@PNCs nanocomposite material were added to hexane, and the mixture was magnetically stirred (1000 rpm) for 30 min to obtain a 2 wt. % homogeneous dispersion. The HSNPs@PNCs nanocomposite suspension was spray coated onto vertically placed substrates (glass, fabric, and aluminum) using a spray-coater with a nozzle diameter of 0.35 mm at a pressure of 4 bar. The coated substrates were dried at room temperature prior to further usage.

2.6. Characterization

The morphology and size of the particles were observed with the FEI Tecnai G2 F20 S-TWIN high resolution transmission electron microscope (TEM) at 200 kV. The crystallinity of PNCs, HSNPs and HSNPs@PNCs were determined by XRD (Panalytical Empyrean). Photoluminescence (PL) and absorbance spectra were measured using an Agilent-Cary Eclipse fluorescence spectrophotometer and Thermo Genesys 10S spectrometer, respectively. Time dependent single photon counting measurements were made using PicoQuant FluoTime 200 equipped with a 375 nm pulsed laser diode. The wettability properties of PNCs and HSNPs@PNCs were evaluated with Attension Theta Lite. Contact angle and sliding angle were measured with 5 μL and 10 μL water droplets, respectively. The chemical composition of the coatings was

characterized using FTIR using the ATR mode (LUMOS II, Bruker).

2.7. Stability tests

Water resistance, thermal treatment, air, and UV light stability tests were performed on the HSNPs@PNCs. In the water stability test, the QY was determined by immersing the composite material in water for 30 days and subjecting it to continuous mixing. The thermal stability test was conducted on the glass substrates coated with HSNPs@PNCs. The substrate was heated on a hot plate at different temperatures (70 °C, 120 °C and 170 °C) for 5 min. In an additional thermal stability test, the substrate was heated at 70 °C for 48 h. To determine the long-term air stability, the HSNPs@PNCs powders were kept in room conditions for 16 days. To investigate photostability, HSNPs@PNCs composites were exposed to a constant luminous flux with a peak wavelength of 397 nm using a 3 mW UV flashlight.

3. Result and discussion

Our approach to fabricate water resistant and stable HSNPs@PNCs is summarized in Fig. 1. PNCs with different halide anions (Cl, Br, I) were synthesized with traditional hot injection method [43]. To impart superhydrophobicity, HSNPs were prepared by coupling of alkylsilane to silica particles. The dispersions of PNCs and HSNPs were then mixed yielding composite materials referred to as HSNPs@PNCs. This dispersion can be deposited on substrates via spray-coating. Also, strong PL brightness of HSNPS@PNCs can be seen when excited with 365 nm UV light.

PL and UV measurements of G-PNCs (green emitting PNCs) are shown in Fig. 2a. G-PNCs emit bright green PL under 365 nm UV light. PL, UV and PLQY a measurements of PNCs and synthesized composites are shown in Table S1 and Fig. S1. PLQY of HSNPs@PNCs can reach to 46 %. Depending on the TEM image in Fig. 2b, G-PNCs have narrow and uniform size distribution. G-PNCs show a cubic shape with an average of 7 nm. HSNPs have a diameter of about 11 nm.

Functionalization of SiO_2 nanoparticles with alkylsilane was confirmed by measuring and comparing the FTIR spectra of SiO_2 and HSNPs (Fig. 2c) The band at 1050 cm^{-1} shows Si-O-Si stretching vibration and represents SiO_2. The peaks around 2850 and 2920 cm^{-1} show C—H stretching vibrations and represent alkylsilane [55]. Elemental composition analysis of SiO_2 nanoparticles functionalized with alkylsilane is shown in Fig. 1d. The carbon atom fraction appears to be 23.2%, which results from the coupling of alkylsilane.

HSNPs@PNCs were imaged in TEM to examine the crystal structure and morphology (Fig. 3a). As shown in Fig. 3b, PNCs were attached to the HSNPs. These black dots (PNCs) appear spherical as they are delimited by the HSNPs surface [17]. For this reason, PNCs look different from their normal appearance. However, the TEM image in Fig. 3c confirms the cubic phase $CsPbBr_3$ plane corresponding to (200) lattice spacing of 0.29 nm. Diffraction peaks of HSNPs@PNCs composites can be seen in XRD patterns (Fig. 3d). HSNPs showed clearly amorphous structure, while PNCs have cubic phase structure. HSNPs showed a wide peak range (16–25) Also, HSNPs@PNCs had amorphous structure and peak range 16–28° XRD results manifested cubic PNCs have characteristic strong peaks 2Θ: 15.1, 21.4, 30.4, 37.6 and 43.6. The peaks refer to 100, 110, 200, 211 and 220 planes based on the standard card of cubic $CsPbBr_3$ phase (PDF#54–0752), respectively. EDX spectra of HSNPs@PNCs were determined the presence of Cs, Pb, Br, Si and O (Fig. 3e). The spectrum affirmed the available elements in PNCs structure. PNCs of halogenic elements (Cl, Br, I) has been successfully mixed with HSNPs, enabling the production of composites with a wide color range. HSNPs indicate no emission in the range of 480–580 nm. In addition, measurements have determined that the dimensions of the composites are relatively narrow. The peak wavelengths of HSNPs intersect exactly with the wavelengths of PNCs in Fig. 3f. This intersection shows that there is no aggregation and reabsorption.

The synthesized composites are shown in Fig. S2 under 365 nm light. The time resolved photoluminescence measurements of PNCs and HSNPs@PNCs are shown in Fig. 3g and Table 1. The average lifetime for HSNPs@PNCs is 10.8 ns while the values of lifetime are 5.5 ns. The synthesized halogenic composites are shown in table S2. These results showed longer lifetime of the PNCs mixed with HSNPs. Thus, HSNPs@PNCs composites can prevent surface passivation. This study showed similar PL lifetime results with hydrophobic PNCs in the literature [14]. For $CsPbBr_3$ PNCs, the shorter lifetime was a few nanoseconds, while the longer lifetime was tens of nanoseconds. The two radiation times τ_1 and τ_2 can be attributed to structural defects such as voids and surface states, respectively. The longer lifespan of τ_3 can be attributed to donor-acceptor transitions [14].

The instability of PNCs under environmental conditions is an important problem that limits their usability. The most important factor limiting the stability is their rapid deterioration in the presence of

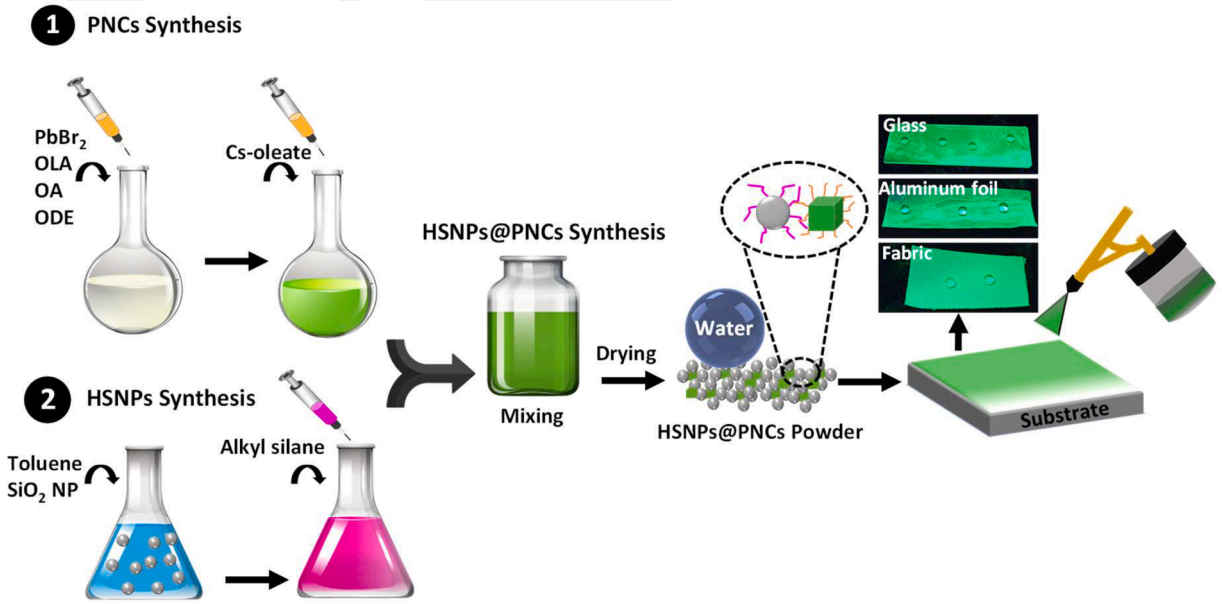

Fig. 1. Schematic illustration for preparation of HSNPs@PNCs.

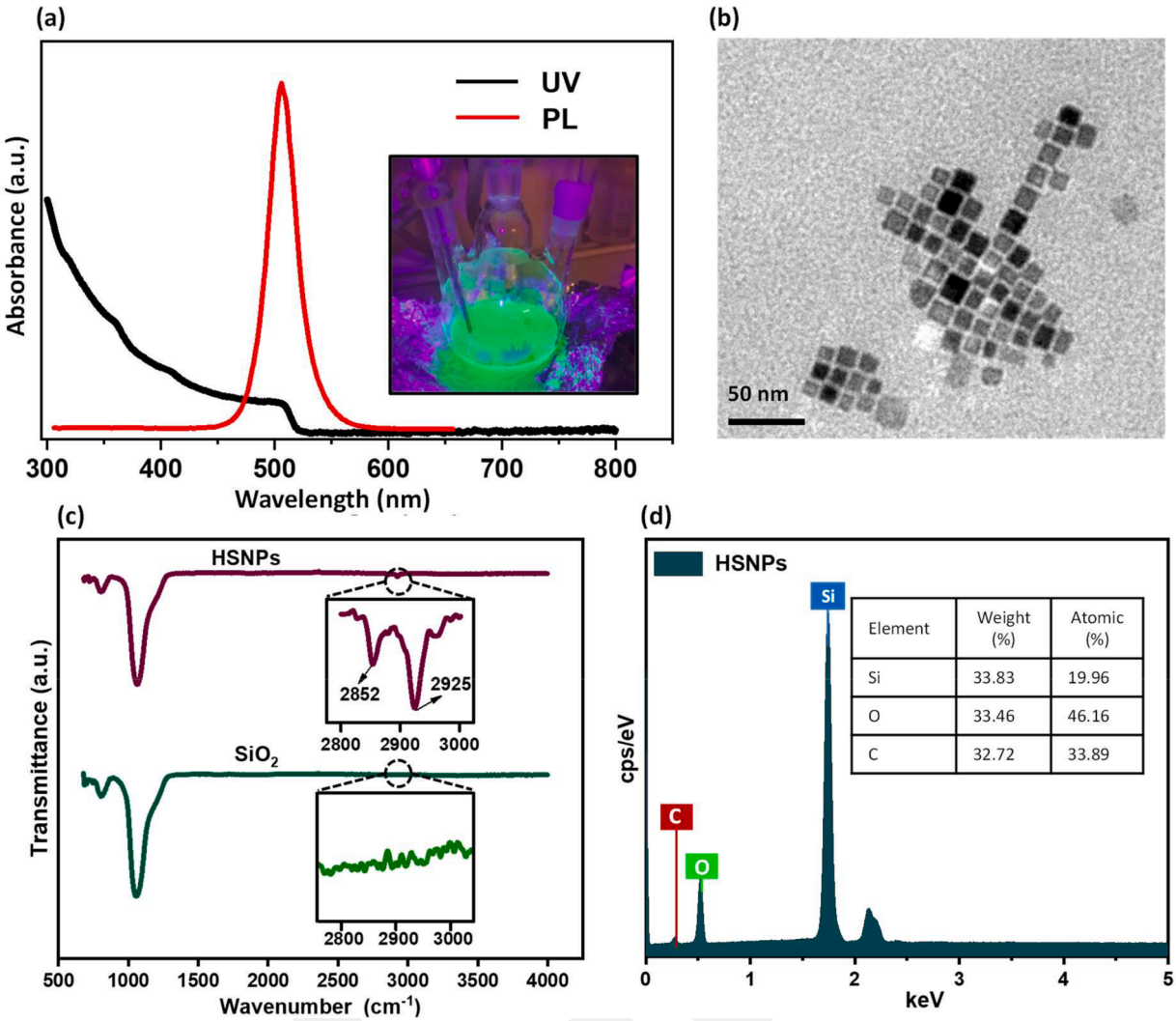

Fig. 2. a) UV and PL spectra. The inset shows the photograph of the PNCs under 365 nm UV light. b) TEM image of the PNCs. c) FTIR spectra of SiO_2 and HSNPs. d) EDX analysis of HSNPs.

moisture. Although the HSNPs@PNCs composite powders we have prepared are known to have superhydrophobic properties, their stability in water is still uncertain. In order to investigate the protective effects of HSNPs, we first started with water stability studies. Water contact angle of PNCs and HSNPs@PNCs are shown Fig. 4a. The water resistance of PNCs is not good, as it is known. HSNPs@PNCs powder materials were suspended in water to investigate their water stability. When HSNPs@PNCs materials were only immersed in water, they immediately floated on the water surface with a clear boundary (Fig. 4a) due to their superhydrophobicity. In addition, the superhydrophobicity of the HSNPs@PNCs composites powder was confirmed by the drop shape analyzer with high contact angles (CA 172°) (Fig. 4a), which is equal to pristine HSNPs. HSNPs@PNCs can be applied homogeneously to different surfaces such as glass, aluminum, and fabric with the spray method (Fig. 4b). The HSNPs@PNCs composite film exhibited high repellent water and strong self-cleaning performances (Fig. 4c and Video S1). Water drops collect coffee particles and move away from the surface.

Given in Fig. 5a, HSNPs@PNCs had 75 % efficiency for 30 days in water stability study, while PNCs lost luminescence properties after immersions water 15 min, which is owing to the destruction of PNCs after high-speed blend (Fig. S3). Further, composite materials showed strong emission even after immersion in water after 6 months. Thus, the superhydrophobic property of HSNPs was also preserved in the prepared HSNPs@PNCs composite materials. It must be known that the CA of the composite materials remained the same even after 6 months. The PL measurements of HSNPs@PNCs (red and blue) against water on a 5-day cycle are 41.1 % and 58.2 %, respectively in Fig. S4. These red and blue luminescent composites have shown to maintain their stability against water by exhibiting superhydrophobic properties. Compared to studies in the literature, it showed superior stability [19]. Not only are PNCs susceptible to oxidation, their stability is greatly impaired at high temperatures. Therefore, it is very important to determine the thermal stability of PNCs. For this reason, PL measurements were taken by exposing PNCs and HSNPs@PNCs to constant and different temperatures. Each temperature value was reserved for 5 min. PL measurements maintain 50 % and 91 % efficiency at 70°, respectively in Fig. 5c. The PL measurements of HSNPs@PNCs at 70 °C, 120 °C and 170 °C are 91 %, 78 % and 30 %, respectively. As can be seen in Fig. 5d, the PL intensity of PNCs decreases severely with high temperature. The main reason for this tremendous decrease is the further decrease of surface ligands with increasing heating [54,56–58].

In contrast, the PL intensity of HSNPs@PNCs slight decrease with high temperature. The PL curves of the PNCs decrease significantly even when exposed to thermal stability in a very short time. However, HSNPs@PNCs can preserve 78 % of their efficiency even at 120°. Therefore, the HSNPs-Si NPs show an important strength in thermal stability of the PNCs. In addition, in typical synthesis methods, PNCs are

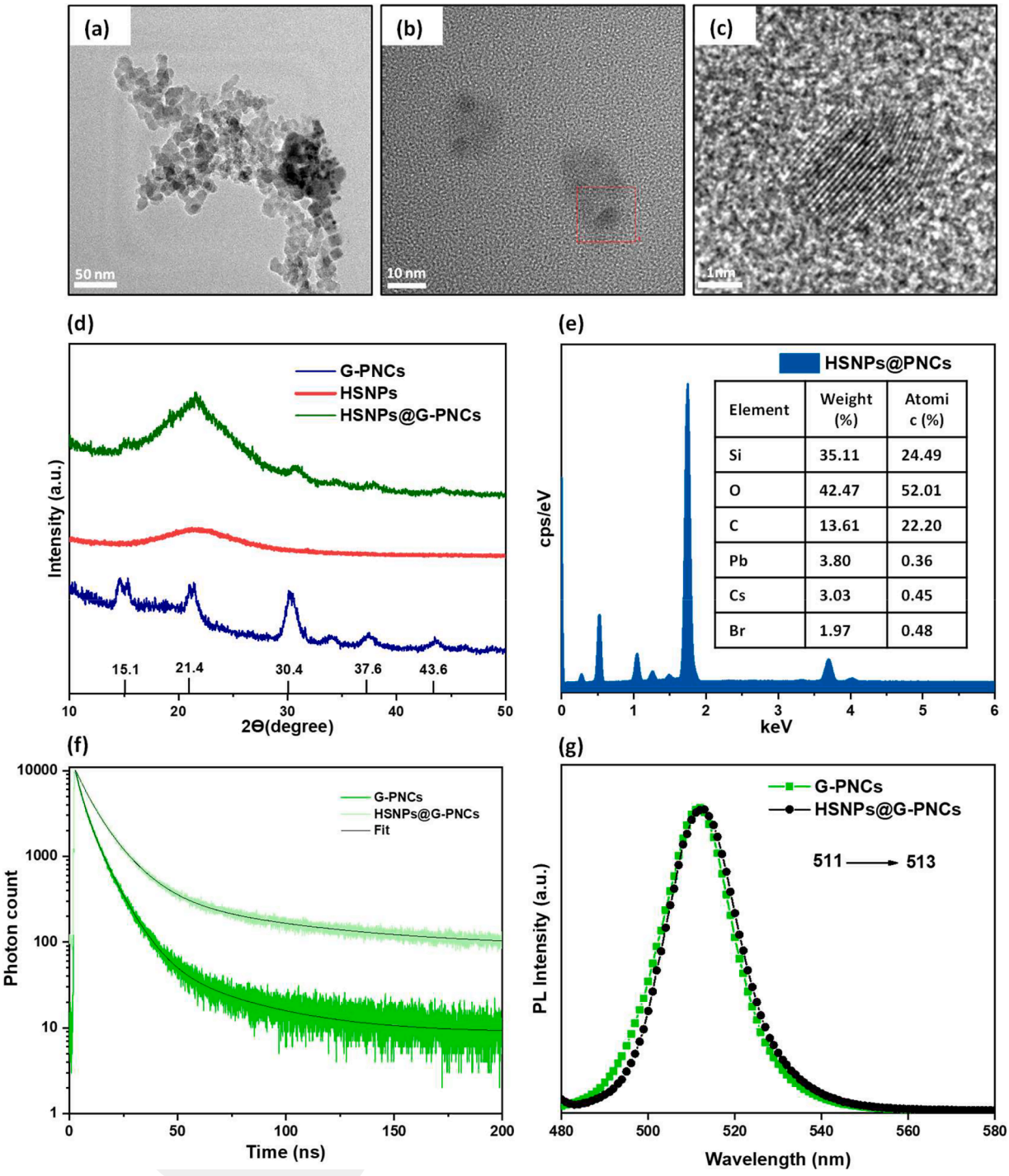

Fig. 3. a-c) TEM image of HSNPs@PNCs d) The XRD patterns of G-PNCs (blue solid line), HSNPs (orange solid line) and HSNPs@PNCs (green solid line) e) The EDX spectra of HSNPs@PNCs. f) TRPL curves of PNCs and HSNPs@PNCs. g) PL spectra of the PNCs and HSNPs@PNCs.

Table 1
TRPL table G-PNCs and HSNPs@G-PNCs.

	PNCs	HSNPs@PNCs
A_1	5998 ± 145	4778.8 ± 58.1
τ_1 (ns)	3.1395 ± 0.0762	12.221 ± 0.119
A_2	98.4 ± 7.35	4756 ± 110
τ_2 (ns)	36.79 ± 1.71	5.603 ± 0.132
A_3	4111.3 ± 60.8	348.73 ± 9.59
τ_3 (ns)	8.3634 ± 0.0859	63.81 ± 1.5
$\tau_{average}$ (ns) (amplitude weighted)	5.5679	10.857

stored in solvent and their stability is weaker in their solid state than in their colloid state. However, since the solvents of PNCs generally have toxic and harmful content, it is recommended to store them in solid form. In this regard, its stability in the air environment is also of great importance. As shown in Fig. 5f, the air stability of HSNPs@PNCs composites worked for 16 days and were preserved 78 % efficiency. The HSNPs@PNCs are irradiated with UV light for 24 h, the composites still exhibites bright green luminescence even after 24 h (Fig. S5). HSNPs were preserve PNCs to against UV light.

The developed HSNPs@PNCs showed excellent performance in different stability tests applied. In addition, when the results in Table 2

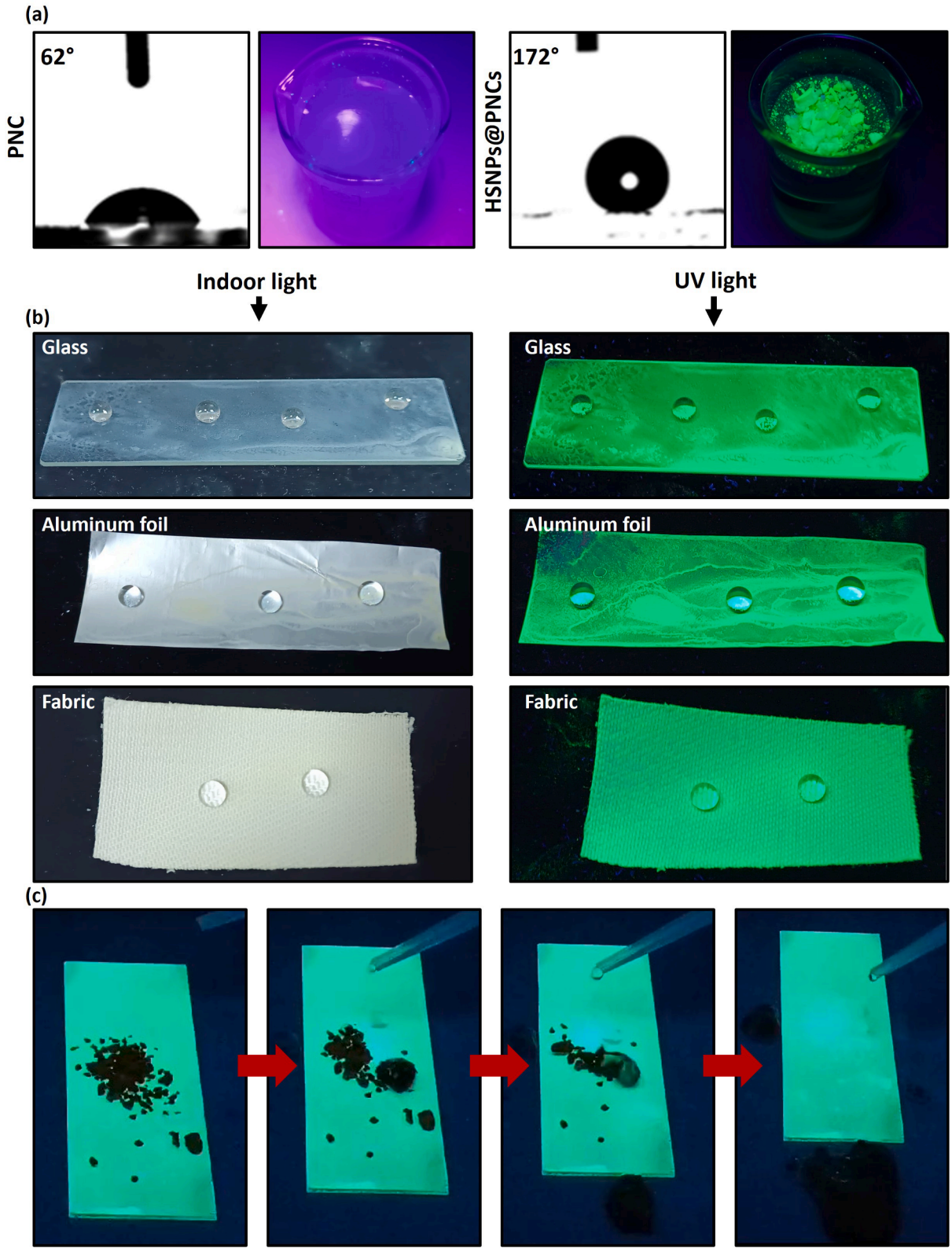

Fig. 4. a) Image of contact angles of G-PNCs and HSNPs@PNCs powder and demonstration of its behavior in water **b)** Normal and UV-light photographs of glass, aluminum foil, and fabric coated with HSNPs@PNCs. **c)** Self-cleaning of coffee particles via rinsing with water.

are examined, it has superior stability and contact angle compared to other studies in the literature.

4. Conclusion

In summary, HSNPs@PNCs nanocomposites were successfully synthesized via a simple method, setting as the visible spectral region of 450

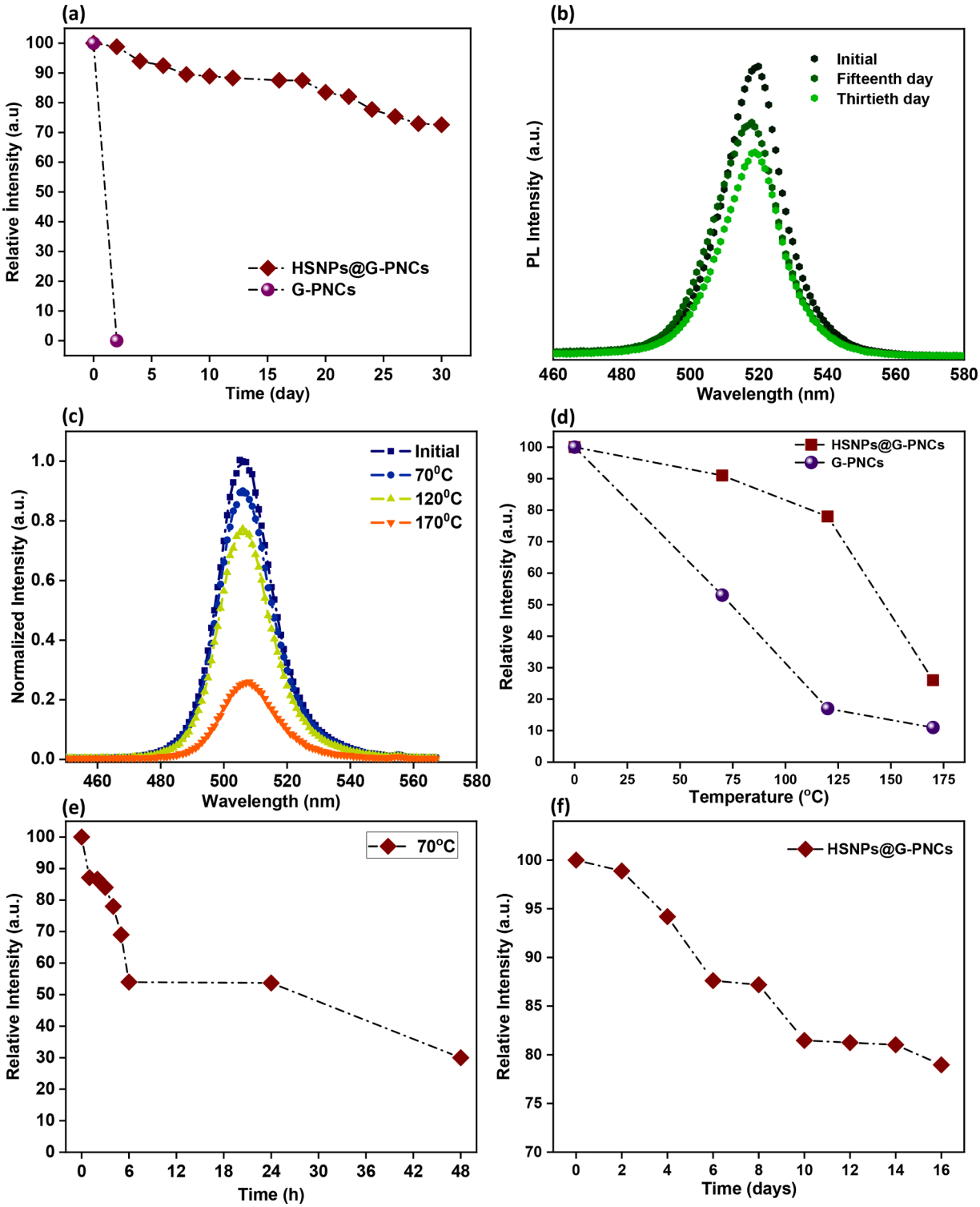

Fig. 5. a) Relative intensity curves of the G-PNC and HSNPs@PNCs composites powder after immersion water for 30 days. b) PL intensity curves of the HSNPs@PNCs composites powder after immersion water for 30 days. c) Normalized intensity curves of the HSNPs@PNCs composites powder as different temperature dependent. d) Relative intensity curves of the G-PNCs and HSNPs@PNCs composites powder as different temperature dependent. e) Relative intensity curves of the HSNPs@PNCs composites powder as continuous at 70 °C. f) Relative intensity curves of the HSNPs@PNCs composites powder air stability after 15 days.

nm - 650 nm without degrading the original structure of PNCs. HSNPs@PNCs composites own PLQY 46 %. Compared with stability related studies of PNCs, HSNPs@PNCs showed evidently developed stability against water exposure, thermal treatment and photostability. The HSNPs@PNCs composite film exhibited very good super-hydrophobic and self-cleaning performances. HSNPs@PNCs composites excellently protected 75% of their initial photoluminescence after being immersed in water for 30 days. Also, the composites manifest high bright emission even after 12 months of room temperature ambient storage. HSNPs@PNCs composites have excellent resistance toward continuous heat treatment as well as different temperatures. The results indicated that HSNPs@PNCs composites has very advantageous of the

Table 2
Comparison of the stability performance with the literature.

Sample	PLQY (%)	Water stability (%, relative)	Air Stability (%, relative)	Thermal Stability (%, relative)	UV stability (%, relative)	Contact Angle (CA)	Reference
CsPbBr/PMSQ AG	57	50 (14 day)	71(15 days)	63 (75 °C)	25 (9 h)	142°	[14]
CPB@SHFW	60	65 (9 days)	–	–	59 (24 h)	150°	[15]
PQD@AGs	66	–	–	70 (50 °C)	100 (5 h)	160°	[54]
CsPbBr3@AGs	71	100 (40 min)	–	148 °C emission	90 (7days)	–	[17]
HSNPs@PNCs	**46**	**75 (30days)**	**78 (16days)**	**91 (70 °C)**	**20**(24 h)	**172°**	**This work**

stability development and long-term durability for different optoelectronic applications, i.e., display technology.

5. Author agreement statement

We the undersigned declare that this manuscript is original, has not been published before and is not currently being considered for publication elsewhere.

We confirm that the manuscript has been read and approved by all named authors and that there are no other persons who satisfied the criteria for authorship but are not listed. We further confirm that the order of authors listed in the manuscript has been approved by all of us.

We understand that the Corresponding Author is the sole contact for the Editorial process.

He/she is responsible for communicating with the other authors about progress, submissions of revisions and final approval of proof.

CRediT authorship contribution statement

Sema Karabel Ocal: Writing – original draft, Methodology, Data curation, Conceptualization. **Nusret Çelik:** . **M. Serdar Onses:** Writing – review & editing, Writing – original draft, Project administration, Methodology, Conceptualization. **Evren Mutlugun:** Writing – review & editing, Writing – original draft, Supervision, Project administration, Methodology, Conceptualization.

Declaration of competing interest

The authors declare the following financial interests/personal relationships which may be considered as potential competing interests:

Evren Mutlugun, M. Serdar Onses reports financial support was provided by Scientific and Technological Research Council of Turkey. Sema Karabel Ocal reports financial support was provided by Scientific and Technological Research Council of Turkey. If there are other authors, they declare that they have no known competing financial interests or personal relationships that could have appeared to influence the work reported in this paper.

Data availability

The data that has been used is confidential.

Supplementary materials

Supplementary material associated with this article can be found, in the online version, at doi:10.1016/j.surfin.2024.103954.

References

[1] W. Deng, L. Huang, X. Xu, X. Zhang, X. Jin, S.T. Lee, J. Jie, Ultrahigh-responsivity photodetectors from perovskite nanowire arrays for sequentially tunable spectral measurement, Nano Lett 17 (4) (2017) 2482–2489, https://doi.org/10.1021/acs.nanolett.7b00166.

[2] Y. Liu, M. Guo, S. Dong, X. Jiao, T. Wang, D. Chen, Room temperature colloidal synthesis of CsPbBr3 nanowires with tunable length, width and composition, J. Mater. Chem. C 6 (29) (2018) 7797–7802, https://doi.org/10.1039/C8TC02636J.

[3] Y. Altintas, I. Torun, A.F. Yazici, E. Beskazak, T. Erdem, M. Serdar Onses, E. Mutlugun, Multiplexed patterning of cesium lead halide perovskite nanocrystals by additive jet printing for efficient white light generation, Chem. Eng. J. 380 (2020) 122493, https://doi.org/10.1016/j.cej.2019.122493.

[4] S.A. Veldhuis, P.P. Boix, N. Yantara, M. Li, T.C. Sum, N. Mathews, S.G. Mhaisalkar, Perovskite materials for light-emitting diodes and lasers, Adv. Mater. 28 (32) (2016) 6804–6834, https://doi.org/10.1002/adma.201600669.

[5] H. Zhu, C.C. Lin, W. Luo, S. Shu, Z. Liu, Y. Liu, J. Kong, E. Ma, Y. Cao, R.S. Liu, X. Chen, Highly efficient non-rare-earth red emitting phosphor for warm white light-emitting diodes, Nat. Commun. 5 (1) (2014) 4312, https://doi.org/10.1038/ncomms5312.

[6] A. Rajagopal, K. Yao, A.K.-Y. Jen, Toward perovskite solar cell commercialization: a perspective and research roadmap based on interfacial engineering, Adv. Mater. 30 (32) (2018) 1800455, https://doi.org/10.1002/adma.201800455.

[7] T. Yang, Y. Zheng, Z. Du, W. Liu, Z. Yang, F. Gao, L. Wang, K.C. Chou, X. Hou, W. Yang, Superior photodetectors based on all-inorganic perovskite CsPbI3 nanorods with ultrafast response and high stability, ACS Nano 12 (2) (2018) 1611–1617, https://doi.org/10.1021/acsnano.7b08201.

[8] X. Chen, D. Li, G. Pan, D. Zhou, W. Xu, J. Zhu, H. Wang, C. Chen, H. Song, All-inorganic perovskite quantum dot/TiO2 inverse opal electrode platform: stable and efficient photoelectrochemical sensing of dopamine under visible irradiation, Nanoscale 10 (22) (2018) 10505–10513, https://doi.org/10.1039/C8NR02115E.

[9] Y. Wang, Q. Lu, F. Li, D. Guan, Y. Bu, Atomic-scale configuration enables fast hydrogen migration for electrocatalysis of acidic hydrogen evolution, Adv. Funct. Mater. 33 (43) (2023) 2213523, https://doi.org/10.1002/adfm.202213523.

[10] Y. Song, H. Kim, J.H. Jang, W. Bai, C. Ye, J. Gu, Y. Bu, Pt3Ni alloy nanoparticle electro-catalysts with unique core-shell structure on oxygen-deficient layered perovskite for solid oxide cells, Adv. Energy Mater. 13 (42) (2023) 2302384, https://doi.org/10.1002/aenm.202302384.

[11] Y. Wang, X. Ge, Q. Lu, W. Bai, C. Ye, Z. Shao, Y. Bu, Accelerated deprotonation with a hydroxy-silicon alkali solid for rechargeable zinc-air batteries, Nat. Commun. 14 (1) (2023) 6968, https://doi.org/10.1038/s41467-023-42728-y.

[12] Wang, R.; Gong, Z.; Jiang, Y.; Huang, S.; Liu, B.; Zhou, G.; Liu, J.M.; Gao, J. Low-cost planar organic small molecules as hole transport materials for high efficient perovskite solar cells. *Surf. Interfaces* 2022, 34, 102307. https://doi.org/10.1016/j.surfin.2022.102307.

[13] G. Liu, Z. Song, X. Gao, Y. Wang, Z. Li, Surface modification of paper substrates by a printed UV curing varnish layer and a transferred transparent PEDOT:PSS electrode for paper-based perovskite light-emitting devices in ambient air, Surf. Interfaces 43 (2023) 103552, https://doi.org/10.1016/j.surfin.2023.103552.

[14] Y.T. Hsieh, Y.F. Lin, W.R. Liu, Enhancing the water resistance and stability of CSPBBR3 perovskite quantum dots for light-emitting-diode applications through encapsulation in waterproof polymethylsilsesquioxane aerogels, ACS Appl. Mater. Interfaces 12 (52) (2020) 58049–58059, https://doi.org/10.1021/acsami.0c18371.

[15] T. Xuan, J. Huang, H. Liu, S. Lou, L. Cao, W. Gan, R.S. Liu, J. Wang, Super-hydrophobic cesium lead halide perovskite quantum dot-polymer composites with high stability and luminescent efficiency for wide color gamut white light-emitting diodes, Chem. Mater. 31 (3) (2019) 1042–1047, https://doi.org/10.1021/acs.chemmater.8b04596.

[16] S. Karabel Ocal, N.B. Kiremitler, A.F. Yazici, N. Celik, E. Mutlugun, M.S. Onses, Natural wax-stabilized perovskite nanocrystals as pen-on-paper inks and doughs, ACS Appl. Nano Mater. (2022), https://doi.org/10.1021/acsanm.2c00224.

[17] Z. Chen, J. Zhao, R. Zeng, X. Liu, B. Zou, W. Xiang, High efficiency fluorescent perovskite quantum dots encapsulated in superhydrophobic silica aerogel for wide color gamut backlight displays, Chem. Eng. J. 433 (2022) 133195, https://doi.org/10.1016/j.cej.2021.133195.

[18] A.N. Singh, S. Kajal, J. Kim, A. Jana, J.Y. Kim, K.S. Kim, Interface engineering driven stabilization of halide perovskites against moisture, heat, and light for optoelectronic applications, Adv. Energy Mater. 10 (30) (2020) 2000768, https://doi.org/10.1002/aenm.202000768.

[19] F. Gao, W. Yang, X. Liu, Y. Li, W. Liu, H. Xu, Y. Liu, Highly stable and luminescent silica-coated perovskite quantum dots at nanoscale-particle level via nonpolar solvent synthesis, Chem. Eng. J. 407 (2021) 128001, https://doi.org/10.1016/j.cej.2020.128001.

[20] S.V. Deshpande, R.A. Bhiungade, M.P. Deshpande, K.K. Pawar, T.S. Bhat, S. K. Kulkarni, A.D. Sheikh, Rapid detoxification of polluted water using ultrastable tio2 encapsulated CsPbBr3 QDs in collected sunlight, Mater. Res. Bull. 142 (2021) 111433, https://doi.org/10.1016/j.materresbull.2021.111433.

[21] S. Kim, M.Y. Cho, I.S. Kim, W.J. Kim, S.H. Park, S. Baek, J.M. Oh, S.W. Kim, Solvent-free aerosol deposition for highly luminescent and thermally stable perovskite-ceramic nanocomposite film, Adv. Mater. Interfaces 6 (13) (2019) 1900359, https://doi.org/10.1002/admi.201900359.

[22] J. Ren, T. Li, X. Zhou, X. Dong, A.V. Shorokhov, M.B. Semenov, V.D. Krevchik, Y. Wang, Encapsulating all-inorganic perovskite quantum dots into mesoporous metal organic frameworks with significantly enhanced stability for optoelectronic applications, Chem. Eng. J. 358 (2019) 30–39, https://doi.org/10.1016/j.cej.2018.09.149.

[23] F. Li, Y. Liu, H. Wang, Q. Zhan, Q. Liu, Z. Xia, Postsynthetic surface trap removal of CsPbX3 (X = Cl, Br, or I) quantum dots via a ZnX2/hexane solution toward an enhanced luminescence quantum yield, Chem. Mater. 30 (23) (2018) 8546–8554, https://doi.org/10.1021/acs.chemmater.8b03442.

[24] Y. Li, Y. Lv, Z. Guo, L. Dong, J. Zheng, C. Chai, N. Chen, Y. Lu, C. Chen, One-step preparation of long-term stable and flexible CsPbBr3 perovskite quantum dots/ethylene vinyl acetate copolymer composite films for white light-emitting diodes, ACS Appl. Mater. Interfaces 10 (18) (2018) 15888–15894, https://doi.org/10.1021/acsami.8b02857.

[25] Y. Wang, J. He, H. Chen, J. Chen, R. Zhu, P. Ma, A. Towers, Y. Lin, A.J. Gesquiere, S.T. Wu, Y.Ultrastable Dong, Highly Luminescent Organic–Inorganic Perovskite–Polymer Composite Films, Adv. Mater. 28 (48) (2016) 10710–10717, https://doi.org/10.1002/adma.201603964.

[26] S.N. Raja, Y. Bekenstein, M.A. Koc, S. Fischer, D. Zhang, L. Lin, R.O. Ritchie, P. Yang, A.P. Alivisatos, Encapsulation of perovskite nanocrystals into macroscale polymer matrices: enhanced stability and polarization, ACS Appl. Mater. Interfaces 8 (51) (2016) 35523–35533, https://doi.org/10.1021/acsami.6b09443.

[27] R. Grisorio, F. Fasulo, A.B. Muñoz-García, M. Pavone, D. Conelli, E. Fanizza, M. Striccoli, I. Allegretta, R. Terzano, N. Margiotta, P. Vivo, G.P. Suranna, In situ formation of zwitterionic ligands: changing the passivation paradigms of CsPbBr3 nanocrystals, Nano Lett. 22 (11) (2022) 4437–4444, https://doi.org/10.1021/acs.nanolett.2c00937.

[28] C. Bathula, A. Jana, R. Soni, M. Naushad, H.S. Kim, Enhanced stability of methylammonium lead bromide perovskite interlaced on cellulose nanofiber, Ceram. Int. 49 (18) (2023) 30886–30891, https://doi.org/10.1016/j.ceramint.2023.07.008.

[29] S.M.H. Qaid, H.M. Ghaithan, B.A. Al-Asbahi, A.S. Aldwayyan, Investigation of the surface passivation effect on the optical properties of CsPbBr3 Perovskite Quantum Dots, Surf. Interfaces 23 (2021) 100948, https://doi.org/10.1016/j.surfin.2021.100948.

[30] W. Lv, L. Li, M. Xu, J. Hong, X. Tang, L. Xu, Y. Wu, R. Zhu, R. Chen, W. Huang, Improving the stability of metal halide perovskite quantum dots by encapsulation, Adv. Mater. 31 (28) (2019) 1900682, https://doi.org/10.1002/adma.201900682.

[31] Y. Wei, X. Deng, Z. Xie, X. Cai, S. Liang, P. Ma, Z. Hou, Z. Cheng, J. Lin, Enhancing the stability of perovskite quantum dots by encapsulation in crosslinked polystyrene beads via a swelling–shrinking strategy toward superior water resistance, Adv. Funct. Mater. 27 (39) (2017) 1703535, https://doi.org/10.1002/adfm.201703535.

[32] S. Ye, J.Y. Sun, Y.H. Han, Y.Y. Zhou, Q.Y. Zhang, Confining Mn2+-doped lead halide perovskite in zeolite-y as ultrastable orange-red phosphor composites for white light-emitting diodes, ACS Appl. Mater. Interfaces 10 (29) (2018) 24656–24664, https://doi.org/10.1021/acsami.8b08342.

[33] A. Loiudice, S. Saris, E. Oveisi, D.T.L. Alexander, R. Buonsanti, CsPbBr3 QD/AlOx inorganic nanocomposites with exceptional stability in water, light, and heat, Angew. Chem. Int. Ed. 56 (36) (2017) 10696–10701, https://doi.org/10.1002/anie.201703703.

[34] Y. Wei, H. Xiao, Z. Xie, S. Liang, S. Liang, X. Cai, S. Huang, A.A. Al Kheraif, H. S. Jang, Z. Cheng, J. Lin, Highly luminescent lead halide perovskite quantum dots in hierarchical caf2 matrices with enhanced stability as phosphors for white light-emitting diodes, Adv. Opt. Mater. 6 (11) (2018) 1701343, https://doi.org/10.1002/adom.201701343.

[35] H.Y. Chou, C.W. Lo, K.P. Chang, W.Y. Shi, C.C. Yen, D.S. Wuu, Synthesis of SiO2-coated perovskite quantum dots for micro-LED display applications, Surf. Interfaces 38 (2023) 102802, https://doi.org/10.1016/j.surfin.2023.102802.

[36] H.C. Wang, S.Y. Lin, A.C. Tang, B.P. Singh, H.C. Tong, C.Y. Chen, Y.C. Lee, T. L. Tsai, R.S. Liu, Mesoporous silica particles integrated with all-inorganic CsPbBr3 perovskite quantum-dot nanocomposites (mp-pqds) with high stability and wide color gamut used for backlight display, Angew. Chem. Int. Ed. 55 (28) (2016) 7924–7929, https://doi.org/10.1002/anie.201603698.

[37] Q. Zhong, M. Cao, H. Hu, D. Yang, M. Chen, P. Li, L. Wu, Q. Zhang, One-Pot Synthesis of Highly Stable CsPbBr3@SiO2 Core–Shell Nanoparticles, ACS Nano 12 (8) (2018) 8579–8587, https://doi.org/10.1021/acsnano.8b04209.

[38] *CsPbBr3@SiO2 core–shell nanoparticle films for superhydrophobic coatings | acs applied nano materials*. https://doi.org/10.1021/acsanm.1c01199 (accessed 2023-03-06).

[39] N. Celik, S. Akay, F. Sahin, G. Sezer, E. Dagasan Bulucu, M. Ruzi, H.J. Butt, M. S. Onses, Sustainable and practical superhydrophobic surfaces via mechanochemical grafting, Adv. Mater. Interfaces 10 (15) (2023) 2300069, https://doi.org/10.1002/admi.202300069.

[40] N. Celik, N.B. Kiremitler, M. Ruzi, M.S. Onses, Waxing the soot: practical fabrication of all-organic superhydrophobic coatings from candle soot and carnauba wax, Prog. Org. Coat. 153 (2021) 106169.

[41] N. Celik, B. Sezen, F. Sahin, A. Ceylan, M. Ruzi, M.S. Onses, Mechanochemical coupling of alkylsilanes to nanoparticles for solvent-free and rapid fabrication of superhydrophobic materials, ACS Appl. Nano Mater 6 (16) (2023) 14921–14930, https://doi.org/10.1021/acsanm.3c02489.

[42] I. Torun, N. Celik, N.B. Kiremitler, X. Huang, M.S. Onses, Fully transparent and superhydrophobic electrodes enabled by soft interfaces, Surf. Interfaces 36 (2023) 102576, https://doi.org/10.1016/j.surfin.2022.102576.

[43] D. Wang, Q. Sun, M.J. Hokkanen, C. Zhang, F.Y. Lin, Q. Liu, S.P. Zhu, T. Zhou, Q. Chang, B. He, Q. Zhou, L. Chen, Z. Wang, R.H.A. Ras, X. Deng, Design of robust superhydrophobic surfaces, Nature 582 (7810) (2020) 55–59, https://doi.org/10.1038/s41586-020-2331-8.

[44] N. Celik, F. Sahin, S.S. Ozel, G. Sezer, N. Gunaltay, M. Ruzi, M.S. Onses, Self-healing of biocompatible superhydrophobic coatings: the interplay of the size and loading of particles, Langmuir (2023), https://doi.org/10.1021/acs.langmuir.2c02795.

[45] N. Celik, S. Altındal, Z. Gozutok, M. Ruzi, M.S. Onses, Effect of fabric texture on the durability of fluorine-free superhydrophobic coatings, J. Coat. Technol. Res. 17 (3) (2020) 785–796, https://doi.org/10.1007/s11998-020-00333-4.

[46] F. Sahin, N. Celik, A. Ceylan, S. Pekdemir, M. Ruzi, M.S. Onses, Antifouling superhydrophobic surfaces with bactericidal and SERS activity, Chem. Eng. J. 431 (2022) 133445.

[47] D. Zang, R. Zhu, W. Zhang, X. Yu, L. Lin, X. Guo, M. Liu, L. Jiang, Corrosion-resistant superhydrophobic coatings on mg alloy surfaces inspired by lotus seedpod, Adv. Funct. Mater. 27 (8) (2017) 1605446, https://doi.org/10.1002/adfm.201605446.

[48] T.M. Schutzius, S. Jung, T. Maitra, P. Eberle, C. Antonini, C. Stamatopoulos, D. Poulikakos, Physics of icing and rational design of surfaces with extraordinary icephobicity, Langmuir 31 (17) (2015) 4807–4821, https://doi.org/10.1021/la502586a.

[49] E.J. Falde, S.T. Yohe, Y.L. Colson, M.W. Grinstaff, Superhydrophobic materials for biomedical applications, Biomaterials 104 (2016) 87–103, https://doi.org/10.1016/j.biomaterials.2016.06.050.

[50] M. Ruzi, N. Celik, M.S. Onses, Superhydrophobic coatings for food packaging applications: a review, Food Packag. Shelf Life 32 (2022) 100823, https://doi.org/10.1016/j.fpsl.2022.100823.

[51] I. Torun, Y. Altintas, A.F. Yazici, E. Mutlugun, M.S. Onses, Solid-state encapsulation and color tuning in films of cesium lead halide perovskite nanocrystals for white light generation, ACS Appl. Nano Mater 2 (3) (2019) 1185–1193, https://doi.org/10.1021/acsanm.8b02030.

[52] C. Wang, R. Chesman, A. S, J. Jasieniak, J, Stabilizing the cubic perovskite phase of CsPbI 3 nanocrystals by using an alkyl phosphinic acid, Chem. Commun. 53 (1) (2017) 232–235, https://doi.org/10.1039/C6CC08282C.

[53] S. Wang, H. Wang, D. Zhang, Y. Dou, W. Li, F. Cao, L. Yin, L. Wang, Z.J. Zhang, J. Zhang, X. Yang, Perovskite nanocrystals-polymer composites with a micro/nano structured superhydrophobic surface for stable and efficient white light-emitting diodes, Chem. Eng. J. 437 (2022) 135303, https://doi.org/10.1016/j.cej.2022.135303.

[54] X. You, J. Wu, Y. Chi, Superhydrophobic silica aerogels encapsulated fluorescent perovskite quantum dots for reversible sensing of SO2 in a 3D-printed gas cell, Anal. Chem. 91 (8) (2019) 5058–5066, https://doi.org/10.1021/acs.analchem.8b05253.

[55] X. Wang, Y. Chai, J. Liu, Formation of highly hydrophobic wood surfaces using silica nanoparticles modified with long-chain alkylsilane, Holzforschung 67 (6) (2013) 667–672, https://doi.org/10.1515/hf-2012-0153.

[56] S. Li, Z. Shi, F. Zhang, L. Wang, Z. Ma, D. Yang, Z. Yao, D. Wu, T.T. Xu, Y. Tian, Y. Zhang, C. Shan, X.J. Li, Sodium doping-enhanced emission efficiency and stability of cspbbr3 nanocrystals for white light-emitting devices, Chem. Mater. 31 (11) (2019) 3917–3928, https://doi.org/10.1021/acs.chemmater.8b05362.

[57] Y. Zhao, C. Riemersma, F. Pietra, R. Koole, C. de Mello Donegá, A. Meijerink, High-temperature luminescence quenching of colloidal quantum dots, ACS Nano 6 (10) (2012) 9058–9067, https://doi.org/10.1021/nn303217q.

[58] R. Grisorio, C.N. Dibenedetto, A. Matuhina, G.K. Grandhi, P. Vivo, E. Fanizza, M. Striccoli, G.P. Suranna, Synthetic control over the surface chemistry of blue-emitting perovskite nanocrystals for photocatalysis, ACS Appl. Nano Mater 6 (9) (2023) 8082–8092, https://doi.org/10.1021/acsanm.3c01645.